A robust eco-compatible microporous iron coordination polymer for CO 2 capture

Marvin Benzaqui, Mohammad Wahiduzzaman, Heng Zhao, Md Rafiul Hasan, Timothy Steenhaut, Ali Saad, Jérôme Marrot, Périne Normand, Jean-Marc Greneche, Nicolas Heymans, et al.

A Robust Eco-compatible Microporous Iron Coordination Polymer for CO_2 capture.

Marvin Benzaqui,[a,b] Mohammad Wahiduzzaman,[c] Heng Zhao,[b] Md Rafiul Hasan,[d,e] Timothy Steenhaut,[f] Ali Saad,[a] Jérôme Marrot,[a] Périne Normand,[g] Jean-Marc Grenèche,[h] Nicolas Heymans,[g] Guy De Weireld,[g] Antoine Tissot,[b] William Shepard,[i] Yaroslav Filinchuk,[f] Sophie Hermans,[f] Florent Carn,[j] Magdalena Manlankowska,[d,e] Carlos Téllez,[d,e] Joaquín Coronas,[d,e] Guillaume Maurin,[c] Nathalie Steunou,[a,b*] Christian Serre.[a,b*]

Iron(III) carboxylate based Metal Organic Frameworks (MOFs) / porous coordination polymers (PCPs) have sparked a high interest owing to their high structural diversity and tunable porosity, excellent stability, tailored functionality as well as their scalability, green synthesis associated with their biocompatible and biodegradable character. Herein, we present a new robust Fe(III) based PCP (labelled MIL-178(Fe)) built up from chains of corner sharing Fe octahedra interconnected by 1,2,4- benzene tricarboxylic acid, delimiting one dimensional narrow pore channels (pore diameter< 4.5 Å) decorated with polar groups (μ_2-OH and -CO_2H functions). These structural and chemical features are suitable for the selective adsorption of CO_2. MIL-178(Fe) was synthesized following a simple, and green protocol in water at near ambient conditions using non-toxic reactants, allowing the production of sub-micrometer sized MIL-178(Fe) particles in large amount (30 g). As shown by single- gas isotherms and CO_2/N_2 co-adsorption experiments as well as molecular simulations, this material exhibits a moderate CO_2 capacity at low pressure but a high CO_2/N_2 selectivity. This is fully consistent with the presence of μ_2-OH groups acting as CO_2 adsorption sites, as revealed from both molecular simulations and *in situ* PXRD experiments. Finally, the good compatibility of this MOF with the elastomer block copolymer Pebax®-3533 allowed the processing of homogeneous and defect-free mixed matrix membranes with a MIL-178(Fe) loading of up to 25 wt% that outperformed pure Pebax®-3533 membranes for CO_2/N_2 separation.

Introduction

Metal organic frameworks (MOFs) and porous coordination polymers (PCPs) are a class of porous crystalline hybrid materials constructed through the coordination of multi-metallic units called secondary building units (SBUs) with organic multitopic ligands.[1,2] They have gained widespread interest due to their high surface area, chemical diversity, unprecedented variability of pore shape/size and topology.[1] Therefore, their physico-chemical properties can be finely tuned, making them promising materials for a myriad of applications including gas storage and separation, heterogeneous catalysis, sensing, biomedicine and so on.[3-7] Remarkable advances have been made toward CO_2 capture and separation by using PCPs, MOFs and MOFs based composites.[4,8-10] One of the main advantages of MOFs over other porous materials is their high CO_2 sorption capacity and high CO_2 affinity.[8-10] This largely stems from their potential high pore volume and large amount of CO_2-philic sites that can be introduced within their backbone. Typically, MOFs can integrate multiple CO_2 adsorption sites, e.g. open metal sites, Lewis basic sites and covalently-bound polar functional groups, that enable to achieve preferential CO_2 adsorption over other gas molecules such as N_2, CH_4 and H_2O.[8-11] In addition, post-synthetic modification has been also employed to introduce novel CO_2 adsorption sites without altering or degrading the MOF structure.[4,8-11]

While remarkable advances have been obtained for using PCPs and MOFs in CO_2 capture and separation, their large scale application in this field would require to overcome some challenges such as the limited chemical and thermal stability of

[a.] *Institut Lavoisier de Versailles, UMR CNRS 8180, Université de Versailles St Quentin en Yvelines, Université Paris Saclay 78000 Versailles, France.*
[b.] *Institut des Matériaux Poreux de Paris, ENS, ESPCI Paris, CNRS, PSL university 75005 Paris, France.*
[c.] *ICGM, Univ. Montpellier, CNRS, ENSCM, Montpellier, France.*
[d.] *Instituto de Nanociencia y Materiales de Aragón (INMA), CSIC-Universidad de Zaragoza, Zaragoza 50018, Spain.*
[e.] *Chemical and Environmental Engineering Department, Universidad de Zaragoza, Zaragoza 50018, Spain.*
[f.] *Institute of Condensed Matter and Nanosciences, Université catholique de Louvain, 1348 Louvain-la-Neuve, Belgium.*
[g.] *Service de Thermodynamique et de Physique Mathématique, Faculté Polytechnique de Mons, Université de Mons 7000 Mons, Belgium.*
[h.] *Institut des Molécules et des Matériaux du Mans, UMR CNRS 6283, Université du Maine, 72085 Le Mans, France.*
[i.] *Synchrotron SOLEIL-UR1, Orme des Merisiers, Saint-Aubin, BP 48, 91192 Gif-sur-Yvette , France.*
[j.] *Laboratoire Matière et Systèmes Complexes (MSC), UMR CNRS 7057, Université Paris Diderot, Bât. Condorcet, 10 rue A. Domon et L. Duquet, 75013 Paris, France.*

† Footnotes relating to the title and/or authors should appear here.

Electronic Supplementary Information (ESI) available: [details of any supplementary information available should be included here]. See DOI: 10.1039/x0xx00000x

some of them, particularly in the presence of harsh contaminants.[8,12] Indeed, numerous MOFs reported so far for CO_2 capture still lack the requisite chemical stability. Note that moisture is a major concern in industrial gas separation as it is not economically feasible to use completely dry feed-gas streams. Therefore, only hydrothermally stable MOFs can be considered for real practical applications. Various strategies have been explored to design stable MOFs by privileging the formation of strong metal -ligand coordination bonds with the use of high valent metal cations (III/IV) according to Pearson's hard/soft acid/base principle, or alternatively the incorporation of hydrophobic and/or polydentate organic linkers.[12,13]

In this context, Fe(III) carboxylates - denoted here "Fe-MOFs"- were thus considered so far since the association of Fe^{3+} cation with strong Lewis acid property and carboxylate ligands can produce, although not systematically, water stable MOFs.[14,15] Moreover, iron is widely distributed in nature and environmentally friendly. The abundance of iron and its low toxicity have promoted the development of Fe-MOFs, not only for gas separation but also for (photo)catalysis, heat reallocation, (bio)sensing or biomedicine due to their good chemical stability, high porosity and biocompatibility.[14,16-19]

So far, Fe(III) MOFs of different architectures, such as the MIL-n (MIL-53, MIL-59, MIL-88, MIL-100, MIL-101) series, the Fe-soc-MOF or $Fe_4(\mu_3\text{-}O)_2(BTB)_{8/3}(DMF)_2(H_2O)_2$ have been designed by assembling either di-, tri-, tetranuclear clusters or Fe-hydroxy chains as SBUs and polycarboxylate aromatic moieties as organic linkers.[18,20-23] Fe(III) sites were also introduced in the organic backbone of MOFs by using Fe(III) porphyrin ligands (PCN-223, PCN-224, PCN-600).[24-26] The Fe(III)-phosphonate MOFs such as Fe-CAU-53 were also recently reported.[27] However, not all of these MOFs exhibit a high hydrolytic stability that is not only driven by the type of SBUs but also the connectivity as well as the size and hydrophobic character of the organic linker.[14-27] As an example, the good hydrothermal stability of MIL-53(Fe) is certainly due to its 1D micropore channel structure based on $[Fe(OH)(COO)_2]_n$ chains while the mesoporous MIL-101(Fe) and PCN-333(Fe) based on the oxo-trimers SBU present a limited water stability. Due to the presence of CO_2 adsorption sites such as Lewis acid Fe^{3+} sites or polar functions (OH, F) and a high pore volume, a few Fe-MOFs such as MIL-100(Fe), MIL-88A(Fe), soc MOF(Fe), Fe-BTB and Fe-BTC have been considered for CO_2 capture and some of them have shown attractive CO_2 uptake at low pressure (> 2 $mmol.g^{-1}$ at 1 bar, 298 K).[14,15,28,29] Recently, a Fe-MOF ($Fe_4(\mu_3\text{-}O)_2(BTB)_{8/3}(DMF)_2(H_2O)_2$), whose structure consists of two interpenetrating 3D skeletons, has shown a greater CO_2 uptake than that of several known MOFs with larger pore volume as a result of its small pore and the presence of multiple CO_2 adsorption sites induced by the framework interpenetration.[23]

Another property of MOFs and PCP that was exploited for CO_2 capture is their propensity for structural flexibility. In particular, a few Fe-MOFs or Fe-PCPs can undergo structural changes such as pore opening upon exposure to stimuli such as pressure or temperature.[30] In such cases, the CO_2 adsorption capacity of these MOFs such as MIL-53(Fe) can drastically increase at a definite gas pressure.[31] Moreover, it was demonstrated that the structural flexibility and thus CO_2 adsorption capacity of MIL-53(Fe) could be modulated through the functionalization of the organic linker of the MOF.[32] It was shown that the CO_2 adsorption capacity of MIL-53(Fe)-X could be enhanced through the introduction of groups with low polarity (X=Cl, Br, CH_3) that could modulate the μ_2-OH/CO_2 interactions instead of directly interacting with CO_2 molecules.[32]

In spite of these interesting results, the number of Fe-MOFs and Fe-PCPs that combine all the properties required for CO_2 separation (high CO_2 adsorption capacity and selectivity, high chemical and thermal stability) is still limited. Moreover, many challenges regarding their synthesis remain unaddressed. Numerous Fe-MOFs are often prepared in the presence of toxic organic solvents and reactants and through solvo/hydrothermal process leading to fine powdered materials made of micron-sized particles.[14,15] This restricts their applications to a great extent. Therefore, the development of Fe(III)-MOFs using safer synthetic conditions allowing both the control of the crystal size and their large-scale production is still an open challenge for their future practical applications.[33]

Herein, we report the synthesis and characterization of a novel PCP based on iron(III) and 1,2,4-benzene tricarboxylate (Fig. 1), named MIL-178(Fe) (MIL stands for Material of Institut Lavoisier) that exhibits a 1D architecture delimiting ultra-micropores (ϕ < 4.5 Å) decorated with functional groups (-COOH, -OH). The structural behavior of this PCP upon CO_2 pressure has been investigated by *in situ* powder X-ray diffraction and molecular modelling, thereby providing a detailed analysis of the preferential arrangement of the confined CO_2 molecules in the material porosity and the host/guest interactions. Finally, co-adsorption CO_2/N_2 experiments and grand canonical Monte Carlo simulations were performed in tandem, revealing that this PCP presents an excellent CO_2/N_2 selectivity. Due to its high hydrothermal stability and scalability under room temperature green conditions, this PCP was used as an inorganic filler for the processing of mixed matrix membranes (MMMs). Its combination with the elastomeric block copolymer Pebax®-3533 led to defect-free composite membranes with an enhanced CO_2/N_2 post-combustion separation performance in comparison to the bare polymer. Pebax®-3533 was preferred over the most studied Pebax®-1657 due to the fact that the former is not water/ethanol soluble. Therefore, Pebax®-3533 based membranes are prone to be more stable in the separation of a realistic humid flue gas.[34]

Experimental

Chemicals.

All chemicals were obtained commercially and used without further purification. The chemicals in this work were anhydrous $FeCl_3$ (Sigma Aldrich 99%), 1,2,4-benzene tricarboxylic acid (1,2,4-BTC) (Sigma Aldrich, 95 %). Pebax® MH 3533 was generously provided by Arkema, France.

Hydrothermal Synthesis of MIL-178(Fe)-*hyd*. Single crystals of MIL-178(Fe)-hyd were synthesized via a

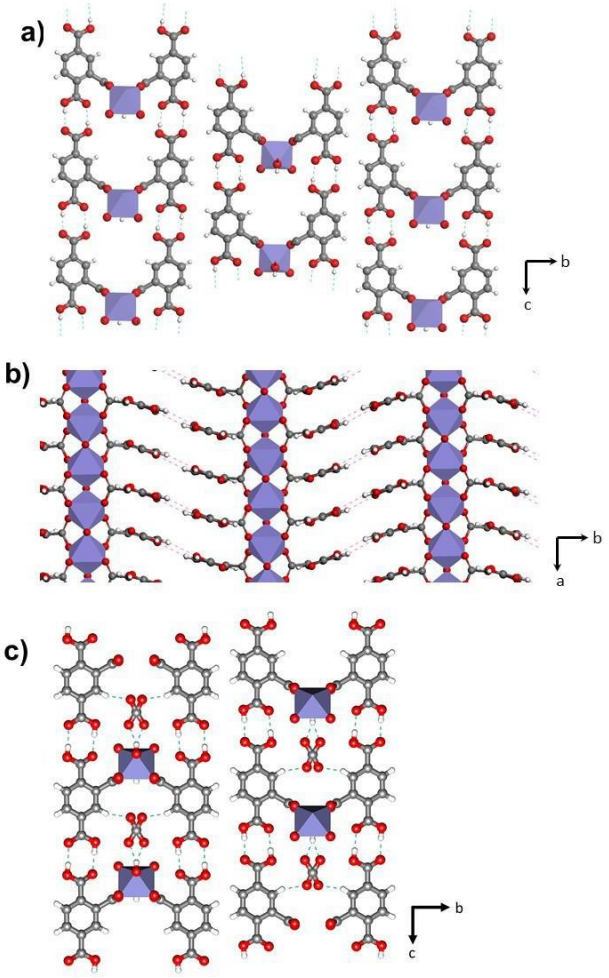

Fig. 1. Crystal Structure of (a,b) MIL-178(Fe) along the (a) a axis and (b) c axis, (c) CO_2 loaded-MIL-178(Fe) along the a axis. Fe octahedral, carbon, oxygen and hydrogen are in purple, gray, red and white respectively. Hydrogen bonds are represented as dotted lines.

hydrothermal route. 1,2,4-BTC (1.15 g, 5.5 mmol) was poured into a 125 mL Teflon-lined steel autoclave with anhydrous $FeCl_3$ (1.29 g, 8 mmol) and 10 mL of deionized H_2O. The mixture was stirred for 10 min and heated to 200°C for 72 h under autogenous pressure. The resulting solution was then filtered and a yellow powder was obtained after extensive washing with water and ethanol to remove the unreacted ligand.

Room temperature synthesis of MIL-178(Fe)-*RT*. 1,2,4-BTC (1.05 g, 5 mmol) and anhydrous $FeCl_3$ (0.81 g, 5 mmol) were poured into a 100 mL beaker with 50 mL of deionized H_2O and stirred at room temperature for 5 days. A bright yellow powder was then recovered by filtration after extensive washings (H_2O & ethanol).For the scale-up synthesis of MIL-178(Fe)-*RT,* 150 mmol of both $FeCl_3$ and 1,2,4-BTC and 1,5 L of water were used.

Fabrication of Mixed Matrix Membrane. The MMMs were prepared following a two-step process. First, 6 wt.% Pebax® MH 3533 (of total weight of 3 g (polymer + solvent)) was dissolved in 1-propanol: 1-butanol (75/25 (v/v)) by stirring under reflux for 1 h. Afterwards, dissolved polymer was used to cast bare polymeric membranes for comparison. In case of MMMs, MIL-178(Fe)-*RT* was dispersed in the dissolved polymer. The required amount of filler (5 wt.% – 25 wt.%) which was calculated against the amount of Pebax® MH 3533 being used, was dispersed in 1.5 mL of 1-propanol/1-butanol (75/25 (v/v)) by repeated sonication and stirring at RT for 1 h. Next, both dispersions were mixed and kept under stirring overnight at RT. In the next step, the solution was poured in a Petri dish. At the end of the process, the membranes were dried for 48 h in a top-drilled box under a solvent-saturated atmosphere under ambient conditions. MMMs are labelled MIL-178(Fe)-Pebax-X where X represents the weight fraction of MIL-178(Fe)-*RT.* MMMs were tested in the CO_2/N_2 separation running both single gas permeability (time lag) and 15/85 CO_2/N_2 mixture measurements. Further details of these experiments are provided in the SI.

Computational Methods. MIL-178(Fe) structure models were optimized at the DFT level with the Quickstep module of the CP2K code using the PBE functional and the triple zeta basis set (TZVP-MOLOPT) for all atoms, except for the Fe centres, where double zeta functions (DZVP-MOLOPT) were employed. Semi-empirical dispersion corrections as implemented in the DFT-D3 method were considered. Force field based grand canonical Monte Carlo (GCMC) simulations were performed at 303 K to assess the single component CO_2 and N_2 and binary mixture of CO_2/N_2 at 15:85 molar compositions in the DFT optimized MIL-178(Fe). The LJ parameters of the MOF atoms were taken from the universal force field (UFF), whereas CO_2 and N_2 molecules were described by the TraPPE potential models. The employed atomic partial charges were derived with Density-Derived Electrostatic and Chemical charges (DDEC) method. Further details of these calculations are provided in the SI.

Adsorption measurements. Pure CO_2 and N_2 adsorption measurements have been performed at 303 K up to 10 bars by gravimetric technique using a high-pressure magnetic suspension balance Rubotherm GmbH.[35,36] CO_2/N_2 co-adsorption measurements were performed on about 10 g of MIL-178(Fe) at 303 K and 1 and 3 bar by using an advanced homemade device that combines a volumetric apparatus and gas chromatography analysis (see SI for more details).

Results and discussion.

Synthesis of MIL-178(Fe) and structure resolution by single crystal X-ray diffraction.

MIL-178(Fe) microcrystals were first synthesized through a hydrothermal route using the 1,2,4-BTC ligand and $FeCl_3$ as iron precursor. We did not consider Fe powder as a precursor due to its oxidation to Fe2+ that may thus lead first to the formation of the two-dimensional iron(II)-1,2,4 BTC phase (MIL-67(Fe)) as previously reported.[37]

This material (i.e., MIL-178(Fe)-*hyd*) was isolated as yellow crystalline powder. SEM images show that MIL-178(Fe) consists of uniform and anisotropic ellipsoidal microcrystals with length and diameter of about 19 and 3 μm (Fig. 2(a)). The crystal structure of MIL-178(Fe) was determined by single crystal X-ray diffraction. Due to the small size of the crystals, the X-ray data acquisition was performed at SOLEIL

synchrotron by using the PROXIMA 2A beamline equipped with a micro-focused beam. MIL-178(Fe) crystallizes in the orthorhombic space group *Pnma* with unit cell parameters of a= 6.930(2) Å, b= 28.420 (6) Å and c= 9.560(2) Å and a unit cell volume of 1882.8(7) Å^3. The associated chemical formula of MIL-178(Fe) is $Fe(OH)[C_9O_6H_5]_2(C_2H_5OH)_{0.5}$. MIL-178(Fe) is made of 1D infinite chains of corner sharing Fe^{3+} octahedra along the *a*-axis (Fig. 1). According to the IUPAC definitions,[38] MIL-178(Fe) can thus be described as 1D coordination polymer due to the presence of repeating coordination entities in one dimension. Each six-coordinated Fe^{3+} is covalently linked to two oxygen atoms of bridging μ_2-OH groups and four oxygen atoms of 1,2,4-BTC linker. The Fe-O distances are ranging between 1.946 and 2.038 Å. Interestingly, only one carboxylate group from the ligand bridges two Fe^{3+} centers holding the 1D chain together, the two other carboxylates being free -COOH groups. The free -COOH groups from two different ligands are facing each other and are thus involved in strong hydrogen bonds connecting the 1,2,4-BTC linkers in the *c* direction. Finally, 1,2,4-BTC linkers coordinated to Fe^{3+} octahedra of different 1D chains are also interacting through hydrogen bonds in the *b*-direction. Remarkably, this structure possesses 1D very narrow channels following the *a*-axis, i.e. along the Fe infinite chains, that are occupied by ethanol molecules (Fig. 1). The dimensions of these channels of 3.5 Å * 4.3 Å (see Fig. S8) lie in the range of the CO_2 kinetic diameter (3.3 Å), thereby suggesting that this material is of potential interest for CO_2 capture. Although the structure of MIL-178(Fe) presents free carboxylic acid groups, they are not exposed to the center of pores and may not strongly interact with adsorbed CO_2 molecules. However, the μ_2-OH groups linked to Fe^{3+} octahedra decorate the internal surface of the channels and are known to be preferential adsorption sites for CO_2. MIL-178(Fe)-*hyd* was then characterized by ^{57}Fe Mössbauer spectrometry (Fig. S1). The ^{57}Fe Mössbauer spectra of MIL-178(Fe)-*hyd* at 300 and 77 K display a doublet that consists of two quadrupolar components Γ_1 and Γ_2 with relative amount of 83 and 17% respectively according to the total absorption area. The hyperfine parameters of such components are consistent with high spin Fe^{3+} species in octahedral environment. The ^{57}Fe Mössbauer spectra at 300 and 77 K obtained after evacuating and heating the MIL-178(Fe)-*hyd* sample at 60 and 100°C (Fig. S1) showed only the single quadrupolar Γ_1 component (see SI for more details) while the spectra of the rehydrated MIL-178(Fe)-*hyd* sample are identical to that of the as-synthesized MIL-178(Fe)-*hyd*. According to these experiments, it can be inferred that both components can be assigned to six-fold coordinated Fe^{3+} centers with identical first coordination shell (1,2,4-BTC and μ_2-OH groups) but different second coordination shell. In contrast to the non-hydrated Fe^{3+} site of the major Γ_1 component, the local environment of the Fe^{3+} site of the minor Γ_2 component contains water molecules that are located in the porosity of this

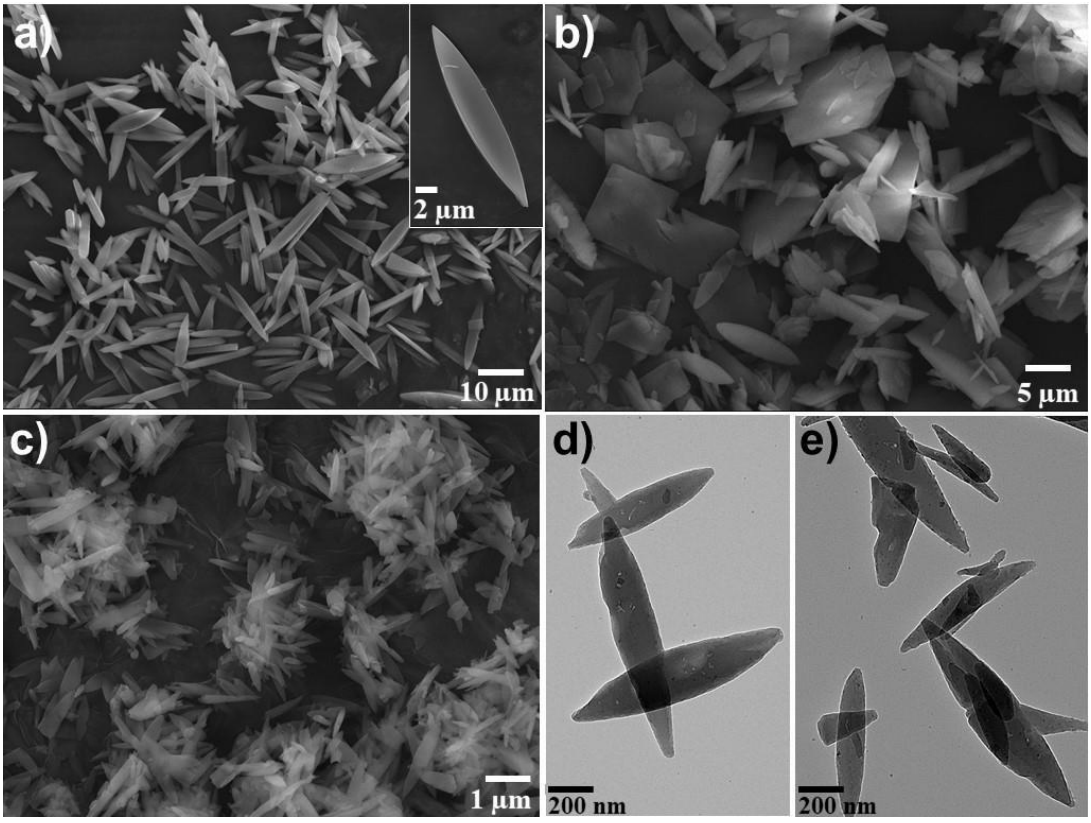

Fig. 2. SEM images of (a) MIL-178(Fe)-*hyd*. The inset shows a higher magnification image of MIL-178(Fe)-*hyd*, (b) MIL-178(Fe)-*re*, (c) MIL-178(Fe)-*RT*, (d-e), TEM images of MIL-178(Fe)-*RT*.

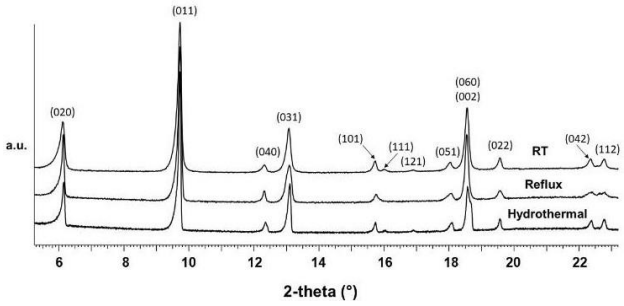

Fig. 3. Powder X-ray diffraction patterns of MIL-178(Fe) synthesized through a hydrothermal process (i.e. MIL-178(Fe)-hyd), under reflux (i.e. MIL-178(Fe)-re) or at room temperature (RT) ((i.e. MIL-178(Fe)-RT).

material. Similar results were previously reported for MIL-82(Fe).[39] MIL-178(Fe) was also characterized by thermogravimetric analyses (TGA) under O_2 (Fig. S2). The first weight loss from 25°C to 200°C corresponds to the removal of free water and ethanol trapped in the pores. The second weight loss between 200 and 400°C follows a two steps process and corresponds to the degradation of the framework. The residual Fe_2O_3 content obtained at 400 °C (~15 wt%) is consistent with the chemical formula $Fe(OH)[C_9O_6H_5]_2(C_2H_5OH)_{0.5}$. Temperature-dependent PXRD experiments were performed thereby confirming that MIL-178(Fe) is stable up to 200 °C (Fig. S3). Moreover, the absence of any XRD peak shift upon increasing the temperature indicates that the framework of MIL-178(Fe) remains somehow rigid under these conditions. The FT-IR spectrum of MIL-178(Fe) shows the characteristic vibration bands of the coordinating carboxylate functions of 1,2,4-BTC (i. e. ν_s(C=O) = 1400 cm^{-1} and ν_{as}(C=O) = 1543 cm^{-1}) and free carboxylate functions at 1703 cm^{-1} (Fig. S4). Temperature-dependent FT-IR spectra of MIL-178(Fe)-hyd were recorded (Fig. S4), showing the progressive increase of two vibration bands at 1852 and 1783 cm^{-1} from 125°C to 225°C. These two bands at 1852 and 1783 cm^{-1} can be respectively assigned to the asymmetric and symmetric carbonyl groups of strained anhydride. The concomitant decrease of the vibration band of the free $–CO_2H$ group at 1703 cm^{-1} upon increasing the temperature is in agreement with the condensation of the free carboxylic acid groups into anhydride. Such phenomenon was previously reported for other MOFs bearing pending $–CO_2H$ group grafted in the organic linkers such as UiO-66(Zr)-(CO_2H) and UiO-66(Zr)-$(CO_2H)_2$.[40] According to temperature-dependent PXRD experiments, the formation of anhydrides does not provoke any structural phase transition. Finally, the hydrothermal stability of MIL-178(Fe) was assessed by heating the material under reflux in deionized water for 72 h. The PXRD and TGA analyses of the hydrothermally treated MIL-178(Fe) are comparable to that of the initial MIL-178(Fe) (see Fig. S5). These results show that MIL-178(Fe) presents a high chemical stability under hydrothermal conditions and does not show any significant flexibility upon water adsorption. Such a strong stability (chemical, thermal) was to our opinion rather unexpected as 1D coordination polymers are often thermally unstable and/or suffer from structural collapse upon desolvation while 3D chains related compounds such as MIL-53(Fe) exhibit a higher hydrothermal stability.[12] Most likely the strong hydrogen bonds between the free –COOH groups leads to stabilization of the framework. The excellent stability of MIL-178(Fe) is therefore of outmost importance for the further practical use of this material for post-combustion CO_2/N_2 separation.

Scale up and control over the particle size of MIL-178(Fe).

The synthetic conditions were then transferred to reflux synthesis in water to tune the crystal sizes of MIL-178(Fe) and enable a multigram scale-up of this material. MIL-178(Fe) could be obtained after heating an aqueous solution of $FeCl_3$ and 1,2,4-BTC under reflux (~ 100 °C) for 16h (see SI for details). The PXRD pattern of this phase (i.e., MIL-178(Fe)-*re*) and TGA analysis are fully consistent with that of MIL-178(Fe)-*hyd* (Fig. 3 and S2). The SEM images of MIL-178(Fe)-*re* show the presence of particles with a high polydispersity in diameter and shape (Fig. 2b). Ellipsoidal particles with the characteristic shape of MIL-178(Fe)-*hyd* are observed but are much smaller with a maximum length of about 5 μm and diameter of about 3 μm. In addition, micrometer-sized platelets of about 5 x 5 μm are also obtained. Room temperature synthesis was then further explored to form particles with a lower diameter and a narrow particle size distribution. After stirring at room temperature an aqueous solution of $FeCl_3$ and 1,2,4-BTC for 5 days, a bright yellow powder (i. e. MIL-178(Fe)-*RT*) was obtained with a good yield (m = 1 g; Yield of 81 % based on Fe). The PXRD pattern of MIL-178(Fe)-*RT* displays the characteristic Bragg peaks of MIL-178(Fe) but as expected are broader in comparison to those of 178(Fe)-*hyd* (Fig. 3). As shown by SEM and TEM, MIL-178(Fe)-*RT* consists of sub-micrometer-sized elongated platelet crystals with a narrow size distribution (Fig. 2(c-e)). Their mean length, diameter and thickness of about 1 μm, 200 and 20 nm respectively are significantly lower than that of MIL-178(Fe) obtained at higher temperatures. Following this synthetic route, MIL-178(Fe)-*RT* could be produced at large scale (e.g., 30 g in one batch with yield of 80% based on Fe) by increasing the amount of precursors and the solvent volume by about 30 times.

CO_2/N_2 Gas Sorption Properties of MIL-178(Fe): Single-Gas Adsorption, *in situ* PXRD, CO_2/N_2 Coadsorption, and Molecular Simulations.

The adsorption properties of this material were investigated. According to TGA (Fig. S2), MIL-178(Fe)-*RT* needs to be activated by outgassing the sample to around 383 K in order to remove all the free water or residual ethanol. Single gas adsorption experiments were first performed on MIL-178(Fe)-*RT* samples. According to N_2 sorption at 77 K (Fig. S6), MIL-178(Fe)-*RT* presents very small N_2 uptake at 77 K which is consistent with the theoretically calculated small pore volume of 0.18 cm^3/g and pore dimensions (< 4.5 Å) of the cavities vs the kinetic diameter of N_2 (3.64 Å). This PCP not only exhibits

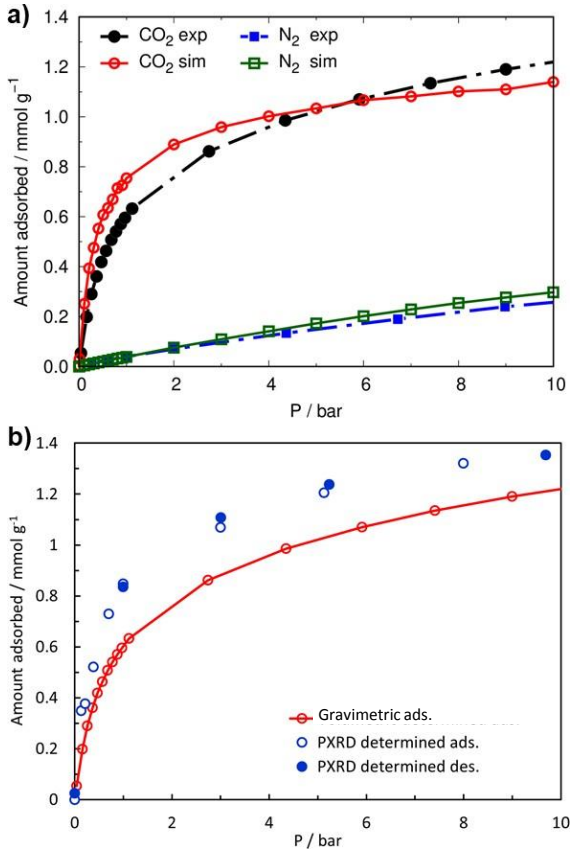

Fig. 4. (a) GCMC calculated and experimental adsorption isotherms for the single components CO_2 and N_2 in MIL-178(Fe)-*RT* at 303 K.(b) PXRD determined adsorption-desorption CO_2 isotherms of MIL-178(Fe)-*RT* in comparison to the experimental adsorption CO_2 isotherm.

very small pore apertures but also presents a good chemical stability and a framework bearing CO_2 adsorption sites (OH groups). It was thus further envisaged to address the CO_2/N_2 post-combustion separation. Fig. 4 shows adsorption isotherms of single gas components CO_2 and N_2 obtained at 303 K. Both isotherms are of Type I with a steeper slope at low pressure for CO_2 as compared to N_2. The N_2 amount adsorbed in MIL-178(Fe) is low with a saturation capacity of 0.25 mmol.g^{-1} at 10 bar. For CO_2, the adsorption uptakes are 0.6 mmol.g^{-1} and 1.2 mmol.g^{-1} at 1 bar and 10 bar respectively. Grand canonical Monte Carlo (GCMC) simulations were further carried out to confirm this experimental trend (see SI for details). As shown in Fig. 4a, the calculated single component CO_2 and N_2 isotherms reproduce well the experimental isotherms at low pressure (<6 bar). The consideration of a fully rigid framework in our GCMC

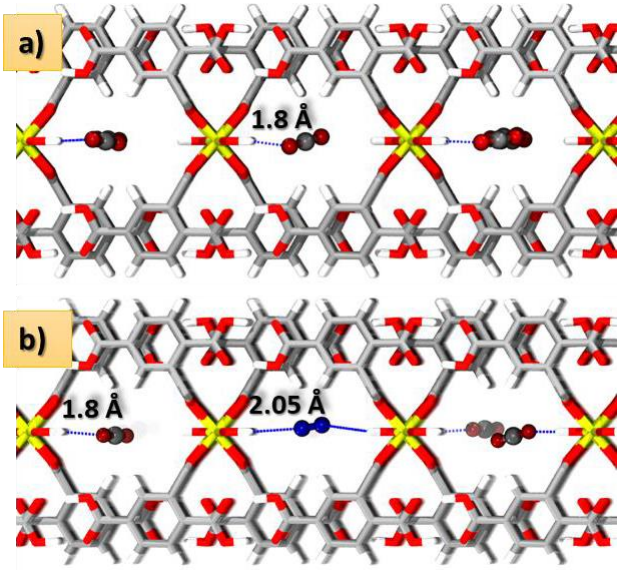

Fig. 5. Microscopic view of the GCMC derived preferential sittings at low pressure for (a) CO_2 molecules as single components and (b) both CO_2 and N_2 molecules in binary mixture in the 1-D channel of MIL-178(Fe).

calculations cannot however capture the experimentally observed gradual increment of uptake amount over higher pressure range. GCMC derived snapshots of the spatial arrangements of the adsorbed CO_2 and N_2 molecules at low pressure (Fig. 5a and Fig. S10) show that μ_2-OH groups act as primary adsorption sites for both CO_2 and N_2 molecules. However, the corresponding radial distribution functions (RDFs) reported in the Fig. S9 clearly indicate that CO_2 molecules interact much more strongly with the μ_2-OH groups compared to N_2 molecules as evidenced by a shorter mean $O(CO_2)\cdots H(\mu_2\text{-}OH)$ distance of 1.8 Å while the $N(N_2)\cdots H(\mu_2\text{-}OH)$ mean distance is 2.05 Å. This preferential geometry is at the origin of a simulated adsorption enthalpy at low coverage for CO_2 (35 kJ.mol^{-1}) much higher than the value obtained for N_2 (20 kJ.mol^{-1}) in line with the experimental adsorption isotherm profiles observed at low pressure. Note that such a moderate adsorption enthalpy is prone to induce an easy reversibility of adsorption–desorption cycles. This is highly desirable for the adsorbent regeneration process as a balance between separation performance and energy cost is required in real adsorption processes. *In situ* PXRD experiments were then performed for various CO_2 pressures up to 10 bar in order to shed light on the possible structural changes of MIL-178(Fe) upon CO_2 adsorption. The whole patterns do not exhibit any drastic modification upon increasing partial pressure of CO_2

with Bragg peaks showing only an intensity change. This indicates that the overall framework of the material is maintained upon loading with CO_2. A model of the MIL-178(Fe) with empty pores was therefore created through the Fox simulated annealing software[41] by starting from the structure solved from single crystal X-ray diffraction in which the solvent molecules were removed. CO_2 molecules were added and their positions optimized by using the pattern obtained under the highest CO_2 pressure. Once the position of CO_2 and occupancy at this loading were determined, Rietveld refinement was conducted using the Fullprof/Winplotr software (see SI for details).[42] Sequential Rietveld refinement was then performed at all the experimental CO_2 pressures. On the basis of these *in situ* PXRD data, adsorption/desorption CO_2 isotherms were calculated and compared to gravimetric sorption data (see Fig. 4(b)). The good fit at each pressure point suggests that the CO_2 molecules are progressively filling the pores without a major change of the host structure or a reorientation of the ligand. Diffraction data suggest that the saturation with CO_2 is reached slightly above the half-filling of the site and this CO_2 adsorption capacity is slightly higher than that found by gravimetric adsorption isotherm (see Fig. 4). As shown in Fig. 1c, CO_2 molecules could be located in the structure of MIL-178(Fe). The center of the guest CO_2 molecule is located on the mirror plane but the molecules are orientationally disordered outside the plane of symmetry. The closest contacts of CO_2 molecules with the host framework are defined by hydrogen bonds of the hydroxyl group, O(μ_2O)-H…O(C), having H…O distance of about 1.82 Å and O-H…O angle of 149 degree which is fully consistent with the GCMC derived preferential sitting reported in Fig. 5. Since MIL-178(Fe) shows a simulated adsorption enthalpy difference between CO_2 and N_2 of more than 15 kJ.mol^{-1}, it is expected to be attractive for the selective adsorption of CO_2 over N_2. GCMC simulations were thus conducted on the binary mixture with a 15/85 CO_2/N_2 molar composition. The relatively high simulated CO_2/N_2 selectivity value ~80 at 1 bar (see Fig. S11) confirms the promise of this material for CO_2 capture. Fig. 5b shows that the preferential adsorption site of CO_2 in MIL-178(Fe) remains the same for CO_2/N_2 mixture as with the CO_2 single component. This prediction motivated binary mixture adsorption experiments by considering post-combustion CO_2 capture, i.e. for a gas mixture CO_2/N_2 = 10/90 and 15/85 at 1.0 bar and 3.0 bar, i.e. the typical industrial concentration and pressure conditions for the separation of flue gas emitted from power plants. Such real co-adsorption data were rarely reported in the literature.[43] Each mixture point was repeated 3 times giving an average selectivity. A high selectivity value of 116±16 was obtained at 1 bar and 303 K for CO_2/N_2 = 10/90 and increases further to a value of 145±15 by increasing the CO_2 concentration (CO_2/N_2 = 15/85). This selectivity value is comparable or greater than that of numerous well-known MOFs with low CO_2 heat of adsorption studied under the same conditions while it remains lower than that of a few MOFs recently reported (see Table S2). By increasing the pressure to 3 bar, the selectivity values decrease but interestingly remain rather high (i. e. S_{EXP} = 66±5 for CO_2/N_2 = 10/90).

Processing of mixed matrix membrane (MMM) for CO_2/N_2 separation.

Since MIL-178(Fe) particles present a good colloidal stability in 1-propanol and 1-butanol solvents (see Fig S14), MMMs were prepared by dispersing MIL-178(Fe)-*RT* in a solution of Pebax®-3533 in 1-propanol/1-butanol solvents mixture (see Experimental part for details). Pebax®-3533 is a poly(amide-6-*b*-tetramethylene oxide) block copolymer composed of 70% of a rubbery poly(tetramethylene oxide) (PTMO) block with high affinity towards CO_2 molecules and 30% of a glassy polyamide (PA) block providing mechanical strength.[44-46] This polymer has the advantage to be commercially available and soluble in non toxic alcohol solvents. In the past few years, the series of Pebax polymers was used as continuous phase in MMMs owing to their promising separation performances resulting from their structural flexibility and solubility-selective gas separation.[47-55] Moreover, a few rubbery Pebax-MOF MMMs have shown better MOF-polymer interfacial properties in comparison to numerous MMMs based on rigid glassy polymers.[47-55] MIL-178(Fe)-Pebax-X MMMs with different MIL-178(Fe) content (X=5-25 wt%) were fabricated following a two-steps protocol (polymer dissolution and filler dispersion followed by casting), as explained in the experimental section. PXRD patterns of the different MIL-178(Fe)-Pebax-X MMMs display the characteristic Bragg peaks of MIL-178(Fe), the intensity of which increases with the amount of MIL-178(Fe) (Fig. 6). This indicates that the crystalline structure of MIL-178(Fe) is preserved upon their association with the polymer. The PXRD pattern of MMMs display also a broad peak at 2θ = 20° corresponding to the crystalline region of PTMO. FT-IR spectra of MIL-178(Fe)-Pebax-X MMMs (Fig. S15) present the characteristic vibration bands of both MIL-178(Fe) and Pebax®-3533, in agreement with the incorporation of the PCP in the polymer matrix and with the prevalence of the PCP crystallinity upon the MMM preparation. The morphology of the membranes was investigated by SEM. In contrast to pure Pebax®-3533 membrane that presents a smooth and homogeneous surface, the surface of MIL-178-Pebax-10 is rougher due to the embedding of well-dispersed MIL-178(Fe) platelets with a random orientation in the polymer matrix as shown in Fig. S16. However, when the MOF content reached a loading of 15 wt%, the morphology of the MMMs changes drastically. As shown in Fig. 6, the top surface of MIL-178-Pebax-15 is smooth and exhibits a lamellar microstructure. Such layered structuration of the MIL-178-Pebax-15 MMM is also observed on cross-section SEM images and is certainly imparted by the stacking of MIL-178(Fe) platelets parallel to the substrate. A similar morphology was observed for MMM with 25 wt% of MIL-178(Fe)-*RT* (Fig.S16). The thickness of the MMMs lies between 40 and 45 µm. The thermal stability of MIL-178(Fe)-Pebax-X MMMs was evaluated by TGA in comparison to the pure MIL-178(Fe) and bare polymer (see Fig. S17). First, negligible weight loss below 250°C shows the removal of any residual solvent in the MMM. The onset decomposition temperatures of MIL-178(Fe)-Pebax-10 and MIL-178(Fe)-Pebax-15 MMMs is slightly higher than that of pure Pebax®-3533 (~ 220°C for MMM vs. 180°C for neat Pebax®-3533) as a result of

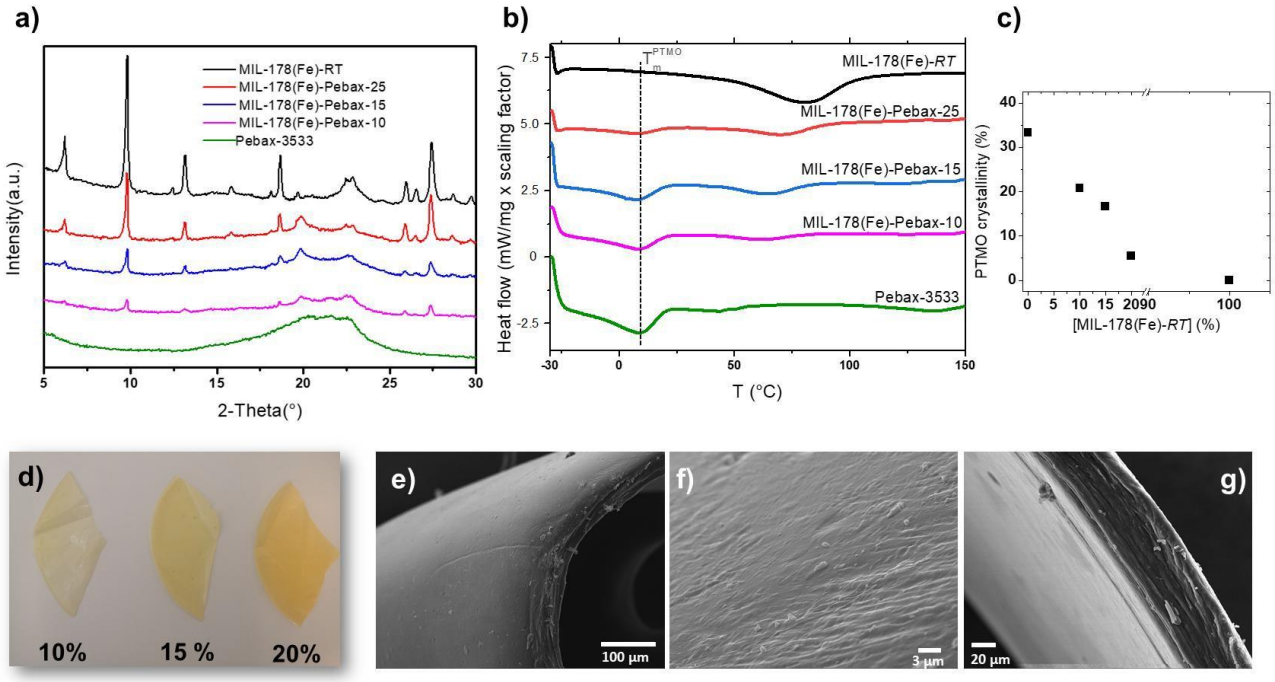

Fig. 6. (a) PXRD of MIL-178(Fe)-Pebax 3533 MMMs in comparison with the pure polymer and MIL-178(Fe)-RT, (b) DSC curves of neat Pebax®-3533 and typical MIL-178(Fe)-Pebax -X MMMs. The curves are shifted vertically for clarity, (c) crystallinity degree of PTMO as a function of the content of MIL-178(Fe)-RT, (d) photographs of MMMs with different MIL-178(Fe) contents. (e,f) SEM images of the top surface and (g) cross-section SEM image of MIL-178-Pebax-15 MMM.

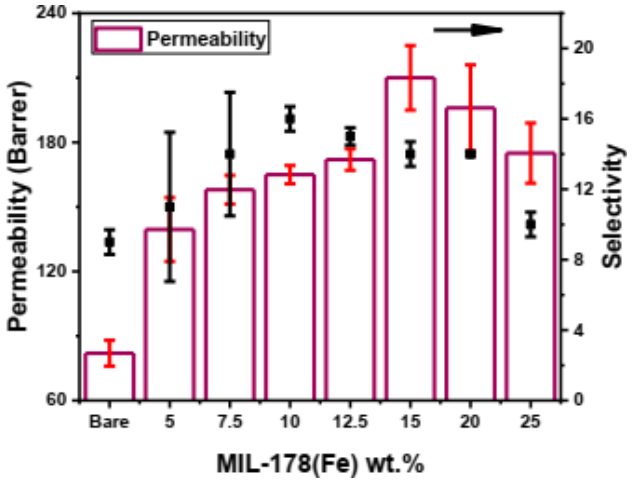

Fig. 7. Permeation analysis of MMMs and their comparison with bare polymer membrane

the good thermal stability of MIL-178(Fe). In contrast, the thermal stability of MIL-178(Fe)-Pebax-25 is significantly lower than that of MMMs with a lower PCP content and pure polymer. This suggests that the interfacial interactions between the PCP and Pebax®-3533 in MIL-178(Fe)-Pebax-25 are presumably lower than that of MIL-178(Fe)-Pebax-X with X=10 and 15. Nevertheless, the overall thermal stability of all MMMs is enough to meet the requirement for CO_2/N_2 separation. The residual amount above 500°C of the MMMs is consistent with their respective MIL-178(Fe) contents. DSC experiments were performed to evaluate the impact of the MIL-178(Fe) filler on the degree of crystallinity of Pebax®-3533.[47] More precisely, as the DSC curves are characterized by a single endothermic peak corresponding to the melting of the PTMO phase (T_m^{PTMO} ~10°C), we have quantified the degree of crystallinity of this phase. This was done for each MMM by calculating the ratio between the enthalpy of fusion (ΔH_f) obtained by integration of the peak and the enthalpy of fusion corresponding to a purely crystalline PTMO phase as obtained from the literature ($\Delta H^* \approx 200\ J_f/g$)[56] (see SI for details). The plot of the crystallinity degree as a function of the MIL-178(Fe)-*RT* concentration shows a continuous decrease from 33% to 5% when the MIL-178(Fe)- *RT* concentration varies from 0 to 20%. Thus, it appears that MIL-178(Fe)-*RT* inhibits the crystallization of the PTMO phase which should favor a significant softening of the Pebax®-3533 considering that this polymer contains 70% of PTMO. Therefore, the addition of MIL-178(Fe) fillers to Pebax-3533 induces the presence of a larger amount of flexible PTMO chains. This is consistent with the mechanical properties of the membranes that were characterized at large deformation by performing tensile tests until failure. Fig. S19 shows the stress-strain curves for the MIL-178(Fe)-Pebax-X MMMs with X=10 and 15 in comparison to the pure Pebax®-3533 matrix. Table S3 provides the values of the Young's modulus (E), the stress at break (σ_{break}) and elongation at break (e_{break}). Compared to the pure Pebax®- 3533 matrix, the mechanical properties of MIL-178(Fe)-Pebax-X MMMs are significantly enhanced. These materials are much

more extensible which is consistent with the presence of a larger amount of rubbery PTMO phase as shown by DSC. Note that the deformability of MIL-178(Fe)-Pebax-15 is slightly lower than that of MIL-178(Fe)-Pebax-10. This can be imparted by the increasing amount of MIL-178(Fe) particles that can act as reinforcing fillers of the polymer as also shown by the higher value of Young's modulus of MIL-178(Fe)-Pebax-15 in comparison to those of the other MMMs. Finally, the long-term chemical stability of the MIL-178(Fe)-Pebax-X MMMs with X=10, 15 and 25 was confirmed by recording PXRD and FT-IR experiments after ageing the composite membranes under humid ambient air for about 8 months, with no evidence of structural evolution (see Fig S20).

Gas separation measurements were carried out by feeding the post-combustion gaseous mixture of CO_2/N_2 (15/85 cm^3(STP) min^{-1}) at an operating pressure of 3 bars to the feed side at 35 °C. A schematic representation of the GC module is given in Fig. S21. Fig. 7 and Table S4 show the CO_2 permeability and CO_2/N_2 selectivity of MIL-178(Fe)-Pebax-X MMMs and pure Pebax®-3533. Remarkably, the addition of MIL-178(Fe) to Pebax®-3533 up to 10 wt% of MIL-178(Fe) led to a significant increase of both the CO_2 permeability and CO_2/N_2 selectivity. The CO_2 permeability of MIL-178(Fe)-Pebax-10 (165 ± 4 Barrer) increased by a factor of 2 compared to the pure Pebax®-3533 (83 ± 6 Barrer) while the CO_2/N_2 selectivity of MIL-178(Fe)-Pebax-10 (16.0 ± 0.7) was improved by about 80% in comparison to the pure polymer (9.0 ± 0.7). Further increase of MIL-178(Fe) content to 15 wt% led to membranes with the highest CO_2 permeability (210 ± 15 Barrer) at the expense of a slight decrease of the CO_2/N_2 selectivity (14.0 ± 0.7). These results indicate that the inclusion of MIL-178(Fe) fillers in the Pebax-3533 matrix can induce a high increase of both permeability and CO_2/N_2 selectivity values up to about 160% and 80% respectively in comparison to the bare membranes. The promising performance of these MMMs can be explained by the high CO_2/N_2 selectivity of the bare MIL-178(Fe) and the good compatibility of the MOF filler with the polymer matrix. Moreover, the ultra-micropores of MIL-178(Fe) are presumably fully accessible to CO2 molecules since the penetration of polymer chains is not likely to occur in the MOF channels (size<4.5 Å). To shed light on the solubility and diffusivity contributions of the gas permeation results, time lag experiments were carried out to obtain CO2 and N2 single gas permeabilities, and subsequently CO2 and N2 diffusivities and solubilities. It is worth to mention that CO2 permeability and CO2/N2 selectivity values of bare membrane and MMM obtained by time lag and mixture separation analyses are in good concordance, as shown in Table S5. Time lag experiments have demonstrated that the inclusion of the MOF in the polymer increases the CO2 solubility (Table S5). CO2 solubility values are 7.3·10-2 and 3.3·10-1 (cm3(STP)/(cm3·cmHg)) for the pure polymer membrane and the MIL-178(Fe)-Pebax-10 MMM, respectively. On the contrary, the CO2 diffusivity decreases (and so does the N2 diffusivity) from the pure polymer to the MIL- 178(Fe)-Pebax-10 MMM from 1.3·10-7 to 3.8·10-8 cm2/s, in agreement with the narrow microporosity of MIL-178(Fe) and the tortuosity created in the MMM by the addition of the filler particles.

Therefore, the enhanced permeability of MMM in comparison to the pure Pebax®-3533 can be partly explained by the increased content of the more permeable amorphous PTMO (lower crystallinity degree) as it was previously reported for a few MOF-Pebax MMMs.[47]

Conclusions

A new water stable 1D microporous coordination polymer, MIL-178(Fe), was discovered, presenting interesting features for CO_2 capture such as hydrothermal and thermal stability as well as ultra-micropores decorated with polar OH groups acting as CO_2 adsorption sites. This material was synthesized through an easily-scalable and environmentally friendly protocol with non-toxic reactants, allowing to achieve the production of a large amount of this material with high yield. Monodisperse MIL-178(Fe) sub-micrometer sized particles were synthesized at room temperature and were used for the preparation of MMMs. The complete characterization of the CO_2/N_2 gas sorption properties of MIL-178(Fe) by combining CO_2/N_2 adsorption/coadsorption experiments, *in situ* CO_2 PXRD and molecular simulations revealed that MIL-178(Fe) presents a moderate CO_2 adsorption capacity at low pressure but retains a high CO_2/N_2 selectivity in the 1-3 bar pressure range due to the high affinity of CO_2 molecules toward μ_2-OH groups located on corner-sharing Fe octahedra chains. MMMs based on MIL-178(Fe) and the Pebax®-3533 elastomer with a PCP loading up to 25 wt% were cast, showing significantly enhanced CO_2/N_2 separation performance in comparison to the pure Pebax®-3533. Such results are likely due to the excellent dispersion of MIL-178(Fe) particles in the polymer matrix with the absence of any interfacial microvoids defects, the enhancement of the MMM CO2 solubility as well as the lower crystallinity degree of the Pebax matrix in comparison to the pure polymer. Finally, its excellent stability and cheap composition makes this PCP of interest for other separation applications as well as sensing or catalysis.[57]

Author Contributions

MB performed the synthesis and characterization of MIL-178(Fe) by PXRD, TGA, FT-IR and N_2 sorption under the supervision of CS and NS. MW and GM performed the molecular simulations. HZ characterized MIL-178(Fe)-RT by TEM and MMMs by PXRD, FT-IR and TGA under the supervision of NS and CS. MRH prepared the MMMs and studied their gas separation properties under the supervision of MM, CT and JC. AS characterized the MMMs by SEM under the supervision of NS. TS, YF and SH performed CO_2 pressure-dependent PXRD experiments and related data analysis. JM, AT and WS characterized MIL-178(Fe) by single-crystal X-ray diffraction. JM determined its crystalline structure. JMG characterized MIL-178(Fe) by ^{57}Fe Mössbauer spectrometry. PN, NH and GDW performed CO_2 and N_2 single gas and co-adsorption experiments. FC characterized MMMs by DSC and performed the tensile tests on the MMMs.

NS wrote the article with the contribution and help of all authors.

Acknowledgements

We acknowledge the European Community Seventh Framework Program (FP7/2007-2013) for funding the research presented in this article under Grant Agreement No. 608490 (Project M4CO2). The computational work was performed using HPC resources from GENCI-CINES (Grant A0100907613).

Conflicts of Interest

There are no conflicts of interest to declare.

Notes and references

[1]Z. Ji, H. Wang, S. Canossa, S. Wuttke, O. M. Yaghi, *Adv. Funct. Mater.*, 2020, **30**, 2000238.
[2]S. Krause, N. Hosono, S. Kitagawa, *Angew. Chem. Int. Ed.,* 2020, **59**, 15325-15341.
[3]D. Zhao, P. K. Thallapally, C. Petit, J. Gascon, *ACS Sustainable Chem. Eng.*, 2019, **7**, 7997-7998.
[4]J. Li, P. M. Bhatt, J. Li, M. Eddaoudi, Y. Liu, *Adv. Mater.*, 2020, **32**, 2002563.
[5]P. Kanti Bharadwaj, P. Feng, S. Kaskel, Q. Xu, *Chem. Asian J.,* 2019, **14**, 3450-3451.
[6]J. W. M. Osterrieth, D.Fairen-Jimenez, *Biotechnol. J.,* 2021, **16**, 2000005.
[7]F. Demir Duman, R. S. Forgan, *J. Mater. Chem. B*, 2021, **9**, 3423–3449.
[8]M. Ding, R. W. Flaig, H. -L. Jiang, O. M. Yaghi, *Chem. Soc. Rev.*, 2019, **48**, 2783–2828.
[9]Z. Hu, Y. Wang, B. B. Shah, D. Zhao, *Adv. Sustainable Syst.*, 2019, **3**, 1800080.
[10]R. L. Siegelman, E. J. Kim, J. R. Long, *Nature Mater.,* 2021, **20**, 1060-1072.
[11]R. Luo, M. Chen, X. Liu,W. Xu, J. Li, B. Liu, Y. Fang, *J. Mater. Chem. A*, 2020, **8**, 18408-18424.
[12]J Duan, W. Jin, S. Kitagawa, *Coord. Chem. Rev.*, 2017, **332**, 48-74.
[13]H. Assi, G. Mouchaham, N. Steunou, T. Devic, C. Serre, *Chem. Soc. Rev.*, 2017, **46**, 3431—3452.
[14]Q. Xia, H. Wang, B. Huang, X. Yuan, J. Zhang, J. Zhang, L. Jiang, T. Xiong, G. Zeng, *Small*, 2019, **15**, 1803088.
[15]S. Zhang, Y. Zhang, F. Baig, T.-F. Liu, *Cryst. Growth Des.*, 2021, **21**, 3100−3122.
[16]A. Permyakova, S. Wang, E. Courbon, F. Nouar, N. Heymans, P. D'Ans, N. Barrier, P. Billemont, G. De Weireld, N. Steunou, M. Frère, C. Serre, *J. Mater. Chem. A*, 2017, **5**, 12889-12898.
[17]S. Cui, M. Qin, A. Marandi, V. Steggles, S. Wang, X. Feng, F. Nouar, C. Serre, *Sci. Rep.,* 2018, **8**, 15284.
[18] S. Patra, S. Sene, C. Mousty, C. Serre, A. Chaussé, L. Legrand, N. Steunou. *ACS Appl. Mater. Interfaces*, 2016, **8**, 20012-20022.
[19]S. Sene, M. T. Marcos-Almaraz, N. Menguy, J. Scola, J. Volatron, R. Rouland, J. -M. Grenèche, S. Miraux, C. Menet, N. Guillou, F. Gazeau, C. Serre, P. Horcajada, N. Steunou, *Chem*, 2017, **3**, 303–322.
[20]C. Serre, C. Mellot-Draznieks, S. Surblé, N. Audebrand, Y. Filinchuk, G. Férey, *Science*, 2007, **315**, 1828-1831.
[21]D. Lenzen, J. G. Eggebrecht, P. G. M. Mileo, D. Fröhlich, S. Henninger, C. Atzori, F. Bonino, A. Lieb, G. Maurin, N. Stock, *Chem. Commun.*, 2020, **56**, 9628-9631.
[22]M. Pang, A. J. Cairns, Y. Liu, Y. Belmabkhout, H. Chun Zeng, M. Eddaoudi, *J. Am. Chem. Soc.*, 2013, **135**, 10234-10237.
[23]S. B. Choi, M. J. Seo, M. Cho, Y. Kim, M. K. Jin, D.-Y. Jung, J.-S. Choi, W.-S. Ahn, J. L. C. Rowsell, J. Kim, *Cryst. Growth Des.*, 2007, **7**, 2290-2293.
[24]D. Feng, Z. -Y. Gu, Y.-P. Chen, J. Park, Z. Wei, Y. Sun, M. Bosch, S. Yuan, H.-C. Zhou, *J. Am. Chem. Soc.,* 2014, **136**, 17714-17717.
[25]D. Feng, W.-C. Chung, Z. Wei, Z.-Y. Gu, H.-L. Jiang, Y.-P. Chen, D. J. Darensbourg, H.-C. Zhou, *J. Am. Chem. Soc.,* 2013, **135**, 17105-17110.
[26]K. Wang, D. Feng, T.-F. Liu, J. Su, S. Yuan, Y.-P. Chen, M. Bosch, X. Zou, H.-C. Zhou, *J. Am. Chem. Soc.*, 2014, **136**, 13983−13986.
[27]F. Steinke, A. Javed, S. Wöhlbrandt, M. Tiemann, N. Stock, *Dalton Trans.*, 2021, **50**, 13572-13579.
[28]S. Wongsakulphasatch, W. Kiatkittipong, J. Saupsor, J. Chaiwiseshphol, P. Piroonlerkgul, V. Parasuk, S. Assabumrungrat, *Greenhouse Gases: Sci. Technol.,* 2017, ***7***, 383-394.
[29]E. Soubeyrand-Lenoir, C. Vagner, J. W. Yoon, P. Bazin, F. Ragon, Y. K. Hwang, C. Serre, J. -S. Chang, P. L. Llewellyn, *J. Am. Chem. Soc.,* 2012, **134**, 10174-10181.
[30]J.-J. Zheng, S. Kusaka, R. Matsuda, S. Kitagawa, S. Sakaki, *J. Am. Chem. Soc.,* 2018, **140**, 13958-13969.
[31]F. Nouar, T. Devic, H. Chevreau, N. Guillou, E. Gibson, G. Clet, M. Daturi, A. Vimont, J. M. Grenèche, M. I. Breeze, R. I. Walton, P. L. Llewellyn, C. Serre, *Chem. Commun.*, 2012, **48**, 10237-10239.
[32]T. Devic, F. Salles, S. Bourrelly, B. Moulin, G. Maurin, P. Horcajada, C. Serre, A. Vimont, J.-C. Lavalley, H. Leclerc, G. Clet, M. Daturi, P. L. Llewellyn, Y. Filinchuk, G. Férey, *J. Mater. Chem.,* 2012, ***22***, 10266
[33]S. Wang, C. Serre; *ACS Sustainable Chem. Eng.,* 2019, **71(4)**, 11911-11927.
[34]A. S. Embaye, L. Martínez-Izquierdo, M. Malankowska, C. Téllez, J. Coronas, *Energy Fuels*, 2021, **35**, 17085-17102.
[35]G. De Weireld, M. Frère, R. Jadot, *Meas. Sci. Technol.,* 1999, **10**, 117.
[36]N. Heymans, S. Vaesen, G. De Weireld, *Micropor. Mesopor. Mater.,* 2012, **154**, 93-99.
[37]M. Riou-Cavellec, C. Lesaint, M. Noguès, J.-M. Grenèche, G. Férey, *Inorg. Chem.*, 2003, **42**, 5669-5674.
[38]S. R. Batten, N. R. Champness, X.-M. Chen, J. Garcia-Martinez, S. Kitagawa, L. Öhrström, M. O'Keeffe, M. Paik Suh, J. Reedijk, *Pure Appl. Chem.,* 2013, **85**, 1715–1724.
[39] M. Sanselme, J.M. Grenèche, M. Riou-Cavellec, G. Férey *Solid State Sci.*, 2004, **6**, 853–858.
[40]F. Ragon, B. Campo, Q. Yang, C. Martineau, A. D. Wiersum, A. Lago, V. Guillerm, C. Hemsley, J. F. Eubank, M. Vishnuvarthan, F. Taulelle, P. Horcajada, A. Vimont, P. L. Llewellyn, M. Daturi, S. Devautour-Vinot, G. Maurin, C. Serre, T. Devic, G. Clet, *J. Mater. Chem. A*, 2015, **3**, 3294–3309
[41]V. Favre-Nicolin, R. Cerny, *J. Appl. Cryst.*, 2002, **35**, 734-743.
[42]J. Rodriguez-Carvajal, *Physica B.*, 1993, **192**, 55-69.
[43]M. Benzaqui, R. S Pillai, A. Sabetghadam, V. Benoit, P. Normand, J. Marrot, N. Menguy, D. Montero, W. Shepard, A. Tissot, C. Martineau-Corcos, C. Sicard, M. Mihaylov, F. Carn, I. Beurroies, P. L. Llewellyn, G. De Weireld, K. Hadjiivanov, J. Gascon, F. Kapteijn, G. Maurin, N. Steunou, C. Serre. *Chem. Mater.,* 2017, **29**, 10326−10338.
[44]L. Martínez-Izquierdo, M. Malankowska, J. Sánchez-Laínez, C. Téllez, J. Coronas, *R. Soc. open sci.*, 2019, **6**, 190866.
[45]L. Wang, Y. Li, S. Li, P. Ji, C. Jiang, *J. Energy Chem.*, 2014, **23**, 717-725.
[46]J. H. Kim, S. Y. Ha, Y. M. Lee, *J. Membr. Sci.* 2001, **190**, 179-193.

[47]S. Meshkat, S.Kaliaguine, D. Rodrigue, *Sep. Purif. Technol.*, 2018, **200**, 177–190
[48]A. Sabetghadam, X. Liu, M. Benzaqui, E. Gkaniatsou, A.Orsi, M. M. Lozinska, C. Sicard, T. Johnson, N. Steunou, P. A. Wright, C. Serre, J. Gascon, F. Kapteijn. Chem. Eur. J., 2018, **24**, 7949 - 7956.
[49]M. Mozafari, R. Abedini, A. Rahimpour, *J. Mater. Chem. A*, 2018, **6**, 12380-12392.
[50]S. Meshkat, S. Kaliaguine, D. Rodrigue, *Sep. Purif. Technol.*, 2020, **235**, 116150
[51]N. Liu, J. Cheng, W. Hou, X. Yang, J. Zhou, *J. Appl. Polym. Sci.*, 2021, **138**, e50553.
[52]J. Shen, G. Liu, K. Huang, Q. Li, K. Guan, Y. Li, W. Jin, *J. Membr. Sci.*, 2016, **513**, 155-165
[53]J. Deng, Z. Dai, J. Hou, L. Deng, *Chem. Mater.*, 2020, **32**, 4174-4184.
[54]N. Habib, Z. Shamair, N. Tara, A.-S. Nizami, F. Hassan Akhtar, N. M. Ahmad, N. Amjad Gilani, M. Roil Bilad, A. Laeeq Khan, *Sep. Purif. Technol.*, 2020, **234**, 116101.
[55]C. Song, R. Li, Z. Fan, Q. Liu, B. Zhang, Y. Kitamura, *Sep. Purif. Technol.*, 2020, **238**, 116500.
[56] I. J. W.Bowman, D. S. Brown, R. E. Wetton, *Polymer*, 1969, **10**, 715-718.
[57]M. Benzaqui, R. Semino, F. Carn, S. Rodrigues Tavares, N. Menguy, M. Giménez-Marqués, E. Bellido, P. Horcajada, T. Berthelot, A. I. Kuzminova, M. E. Dmitrenko, A. V. Penkova, D. Roizard, C. Serre, G. Maurin, and N. Steunou, *ACS Sustainable Chem. Eng.*, 2019, **7**,6629−6639.